Available online at www.sciencedirect.com
ScienceDirect
Microporous and Mesoporous Materials 103 (2007) 57–71
MICROPOROUS AND MESOPOROUS MATERIALS
www.elsevier.com/locate/micromeso

Porous hexacyanocobaltates(III): Role of the metal on the framework properties

J. Roque [a], E. Reguera [a,b,*], J. Balmaseda [a,c], J. Rodríguez-Hernández [a], L. Reguera [d], L.F. del Castillo [c]

[a] Institute of Science and Technology of Materials, University of Havana, 10400 Havana, Cuba
[b] Center for Applied Science and Advanced Technologies of IPN, Mexico, DF, Mexico
[c] Institute of Materials Research, National Autonomous University of Mexico, Mexico, DF, Mexico
[d] Faculty of Chemistry, University of Havana, 10400 Havana, Cuba

Received 17 August 2006; received in revised form 15 January 2007; accepted 17 January 2007
Available online 26 January 2007

Abstract

The extended porous framework of divalent transition metal hexacyanocobaltates(III) was studied from the refined crystal structures and adsorption isotherms of H_2O, CO_2 and N_2. From the obtained adsorption data the pore accessibility, pore volume, adsorption potentials and nature of the guest–host interactions were evaluated. The properties of the porous framework are modulated by the metal used to form the 3D framework from the elemental building block, the hexacyanocobaltate(III) ion. From that fact, this family of microporous compounds can be considered as tunable zeolites, with a pore volume and a system of pore windows appropriate for separation and storage of small molecules. The adsorption isotherms also reveal that the electric field gradient at the pore surface and the pore accessibility are determined by the metal linked at the N end of the CN groups. These compounds are usually obtained as hydrates. The dehydration process and the thermal stability were studied from thermo-gravimetry combined with X-ray diffraction. The crystal water is lost below 100 °C and then the anhydrous structure remains stable, preserving its porous features, up to 250 °C. Upon water removal a progressive cell contraction which amounts 4% of cell volume reduction was observed.
© 2007 Elsevier Inc. All rights reserved.

Keywords: Adsorption; Porous material; Porous structure; Prussian blue analogs; Crystal structure

1. Introduction

Divalent transition metal hexacyanocobaltates(III) form an interesting family of porous molecular materials, with a pore volume and pore windows appropriate for separation and storage of small molecules [1–3]. In this sense, recent studies have evaluated the molecular hydrogen storage in their porous framework [4–6]. Hexacyanometallates can be considered as a 3D assembling of a molecular block, the hexacyanometallate anion, $[M(CN)_6]^{n-}$, through a transition metal cation (T^{m+}), in the following the metal, which links the N ends of neighboring blocks. Within hexacyanometallates, cobalticyanides of divalent cations (T^{2+}), ($T_3[Co(CN)_6]_2 \cdot xH_2O$), are particularly attractive as microporous materials. The Co(III) ion in low spin state has six electrons in the t_{2g} orbitals. These orbitals are filled. This provides a high stability to the building block ($[Co(CN)_6]$). No obvious participation of the hexacyanocobaltate(III) anion in oxidation or reduction processes is expected. The reported hydrogen adsorption isotherms in this family of compounds show certain dependence on the metal involved [4,5], an effect that deserves to be studied since it could be used as a tuning way for the properties of these materials.

Porous cyanometallates are light weight crystalline solids, with a relatively high free volume and with intermediate to

* Corresponding author. Address: Institute of Science and Technology of Materials, University of Havana, 10400 Havana, Cuba. Tel./fax: +53 7 2096653.
E-mail address: ereguera@yahoo.com (E. Reguera).

1387-1811/$ - see front matter © 2007 Elsevier Inc. All rights reserved.
doi:10.1016/j.micromeso.2007.01.030

low adsorption enthalpies for guest species [7,8]. These materials are free of strong polar centers in their structure to provide a high stability to adsorbed molecules through electrostatic interactions, for instance. Such medium intensity guest–host interactions appear appropriate for applications where repeated cycles of adsorption and desorption are required, e.g. in renewable energy sources related technologies. In this sense the studied compounds could be used as prototype of porous materials for such applications.

In the studied family of compounds all the T metals are sited at the pore surface, with the possibility of a direct interaction with the guest molecules within the pores. This fact could be used as a modulation way for the physical properties of the host solid. The guest–host interaction modifies the electronic structure of the solid. For the iron analogues the magnetic properties appear modulated by adsorbed species within the pores [9]. In this sense, the study of the guest–host interactions in hexacyanocobaltates also contributes to shed light on the physical bases of such modulation way for the properties of porous molecular materials. The study of molecular magnets of high temperature of magnetic ordering (T_c) has prompted a renewed interest by hexacyanometallates in the last years [10,11]. The most interesting effects in molecular magnets have been reported for members of this family of coordination compounds, which include the highest T_c values [10,11], photo-induced magnetism [12], humidity induced magnetic pole inversion [13], spin-glass behaviour [14], among others. All these effects have been observed in hexacyanometallates of porous structure.

In this contribution the properties of divalent transition metal hexacyanocobaltate(III), as microporous materials, are evaluated correlating the refined crystal structures with adsorption data using N_2, CO_2 and H_2O as probe molecules. Their dehydration temperatures and thermal stability were studied from thermogravimetry (TG) and X-ray diffraction (XRD). The obtained results shed light on the nature of the metal role in the material porous framework properties. To the best of our knowledge, this is the first study on this subject for this family of materials.

2. Experimental

The studied samples were prepared mixing aqueous solutions (0.01 M) of $K_3[Co(CN)_6]$ and of sulfate of the involved metal (Mn^{2+}, Co^{2+}, Ni^{2+}, Cu^{2+}, Zn^{2+} and Cd^{2+}). The resulting precipitate was aged for a week followed by its separation from the mother liquor by centrifugation. The solid fraction was repeatedly washed with distilled water to remove the accompanying ions and then air-dried until constant weight. The nature of the obtained powders as hexacyanocobaltates(III) was corroborated from infrared (IR) spectra. The atomic metal ratio (T:Co) was estimated by X-ray dispersed-energy spectroscopy analyses. Without exception the obtained T:Co ratio was close to 3:2, in correspondence with the expected formula unit, $T_3[Co(CN)_6]_2 \cdot xH_2O$. The hydration degree ($x$) was calculated from TG curves. The structural characterization was carried out from XRD data. All the reagents used were analytical grade from Sigma–Aldrich.

IR spectra were recorded in an FT-IR spectrophotometer (Genesis Series from Atti Matson) using the KBr pressed disk technique. XRD powder patterns were obtained with CuK_α radiation in an HZG-4 diffractometer (from Carl Zeits) and their preliminary evaluation carried out using program *Dicvol* [15]. The cell contraction on the crystal water removal was evaluated from XRD powder patterns recorded at the X10B beamline of the LNLS synchrotron radiation facility (Campinas, Brazil). The crystal structures were refined from XRD patterns using the Rietveld method implemented in the program *FullProf* [16]. The last refinement stage was performed using program *GSAS* [17] in order to incorporate the diffuse dispersion contribution to the variables to be fitted. TG curves were collected from 25 up to 300 °C, under a N_2 flow (100 mL/min) using a TA instrument thermo-balance (TGA 2950 model) operated in the high-resolution mode. The dehydration process was also studied under vacuum at 10^{-2} Torr in order to select the most appropriate temperature and heating time to obtain anhydrous samples for adsorption experiments.

The adsorption studies were carried out using water vapor, N_2 and CO_2 as probe molecules (adsorbates). The studied compounds have relatively small pore windows (~4.5 Å of diameter) and N_2 and CO_2 appear as appropriate probes to evaluate the pore accessibility. Their kinetic diameters, 3.86 and 3.45 Å, respectively [18], are close to the size of the pore windows. The water molecule is a very informative probe to explore the porous structure of the studied family of compounds. Water is a polar molecule ($\mu = 1.85$ D) of small size (2.65 Å of kinetic diameter) and with a relatively high critical temperature, 374.1 °C [18]. The properties of water are optimal for adsorption studies around room temperature in porous structures with an electric field gradient at the pore surface. In this sense, also ammonia (NH_3) could be used, however, this molecule reacts with the crystal water of cyanometallates inducing their decomposition [19,20].

The N_2 and CO_2 adsorption isotherms were collected at −196 and 0 °C using Accelerated Surface Area and Porosimetry system (ASAP 2010 model from Micromeritic). Water vapor adsorption isotherms were recorded at 30 °C in home made equipment in which water is provided by evaporation from a calibrated capillar and the pressure measured by an oil manometer. Below 30 °C the adsorption kinetics for the water adsorption is very low. With the exception of nickel cobalticyanide, the samples used for adsorption experiments were previously evacuated (10^{-2} Torr) at 80 °C during 4 h. For the Ni salt the dehydration temperature was 105 °C.

The N_2 and H_2O adsorption data were evaluated according to the Dubinin–Astakhov (DA) equation [21]:

$$n_{ad} = n_p \cdot \exp\{-[(R \cdot T/E_0) \cdot \ln(P_r^{-1})]^n\} \quad (1)$$

where n_{ad}: amount adsorbed at a relative pressure $P_r(P_{eq}/P_0)$; n_p: the limiting amount filling the micropores; E_0: characteristic energy; n: the heterogeneity parameter; R: the universal gas constant; and T is the temperature in Kelvin degree. The model was fitted to the experimental isotherms using a non-linear least-squares minimization routine. The starting values of the parameters to be fitted and the fitting region were estimated by plotting the experimental isotherm in Dubinin–Radushkevich coordinates ($n = 2$ in the above DA model). This model has frequently been used for the study of the adsorption in zeolites and carbons [22,23] but also in porous cyanometallates [3,7,24,25].

The CO_2 adsorption data were collected close to the critical temperature for this adsorbate (31 °C) and the obtained isotherms only contain points for relative pressure below 0.03, far from the saturation region. In such conditions the correlation between DA model parameters in non-linear least squares fitting algorithms leads to non-reliable n_p values. An option is to estimate the n_p value using the more general Langmuir–Freundlich (LF) equation based in the solutions thermodynamic, which in its linear form can be expressed as [26]:

$$(1/n_{ad}) = (1/n_p) + (1/(K(P_{eq})^{\beta} n_p)) \quad (2)$$

where K is an affinity parameter that for $\beta = 1$ coincides with the Langmuir constant, P_{eq} is the equilibrium pressure and β is an empirical parameter equivalent to the inverse of the osmotic coefficient in a non-ideal vacancy solution. Then, once the n_p value is known, return to Eq. (1) to calculate the values for the remaining parameters, E_0 and n. Details on this combined application of DA and LF models for the evaluation of adsorption data have been reported elsewhere [3].

For a given adsorbate the studied material compositions were compared according to the variation in the potential (A) on the volumetric pore filling θ (n_{ad}/n_p). The adsorption potential was estimated from the experimental data according to [27,28]:

$$A = R \cdot T \cdot \ln(P_r^{-1}) \quad (3)$$

The pore volume estimation from H_2O, CO_2 and N_2 isotherms was carried out multiplying the respective n_p value by the molar volume in the liquid phase: 18.06 mL/mol for H_2O [18], 42.9 mL/mol for CO_2 [22] and 34.67 mL/mol for N_2 [18].

3. Results and discussion

3.1. Crystal and electronic structure of the studied compounds

As mentioned above, the considered compounds result from a 3 D assembling of the molecular block $[Co(CN)_6]^{3-}$ through the metal (T^{2+}) which links neighboring blocks at their N ends. The charge neutrality forces to a 2:3 block to metal ratio, resulting in materials with the following formula unit $T_3[Co(CN)_6]_2 \cdot xH_2O$. When the metal adopts an octahedral coordination, a highly symmetric structure based on a cubic unit cell is obtained, where 1/3 of the molecular block sites remain vacant. These vacant sites lead to a network of pores (ca. 8.5 Å of diameter) interconnected through small windows, ca. 4.5 Å. These windows are the interstitial free spaces (Fig. 1). In the as-synthesized material the larger pores are filled with water molecules which, can be reversibly removed through the windows without disrupting the material framework. According to the available N sites for the metal, its coordination sphere is formed (in average) by four N atoms plus two water molecules, $T(NC)_4(H_2O)_2$, these last ones contributing to the pore filling. In the formula unit six water molecules are coordinated. The remaining free space within the larger pore is occupied by tightly bound waters (non-coordinated), which are stabilized through hydrogen bonding interactions with the coordinated ones. According to the reported crystal structure for Prussian blue analogues [29], no other types of water or OH group are found in the structure of the studied materials.

Within the studied family of compounds, the crystal structure has been reported for Co [30], Zn [31], and Mn and Cd [32] in a cubic (Fm-3m) unit cell. This is an approximated (average) structural model because the vacant sites lead to certain structural disorder (random vacancies). In that model the metals (Co and T) are sited at (0,0,0) and (0,0,1/2) positions, respectively. However, certain deviations from these ideal sites are expected for both metal centers, mainly for the T atom due to its mixed coordination sphere. The water molecule and the N atom of the CN ligand have different bonding properties. In consequence, the T atom is found to be away from its ideal position (0,0,1/2). From these considerations, the crystal structure for all the studied compounds was refined from the corresponding XRD powder patterns using the Rietveld method, initially in the Fm-3m model and then, in a final refinement stage, abandoning the Wyckoff symmetry restriction for the metal centers. The deviation of the metal centers from their ideal positions leads to a diffuse dispersion contribution to the pattern background. Fig. 2 shows the experimental and fitted XRD powder patterns, and their difference for manganese hexacyanocobaltate(III) and also the mentioned diffuse contribution as a sinuous background (Fig. 2, inset). Such sinuous contribution was incorporated to the variables to be fitted in order to estimate the metals deviation from their ideal sites. The refined atomic positions, and occupation and temperature factors, and other structural details are available as Supplementary Information. In Table 1 the calculated cell edge values, the metal centers position related to the ideal sites, the refinement agreement factors (R), and the estimated crystallite size are collected. According to the calculated unit cell edge for the cubic phases and the reported crystal radius for the metal [33], the pore diameter for the studied

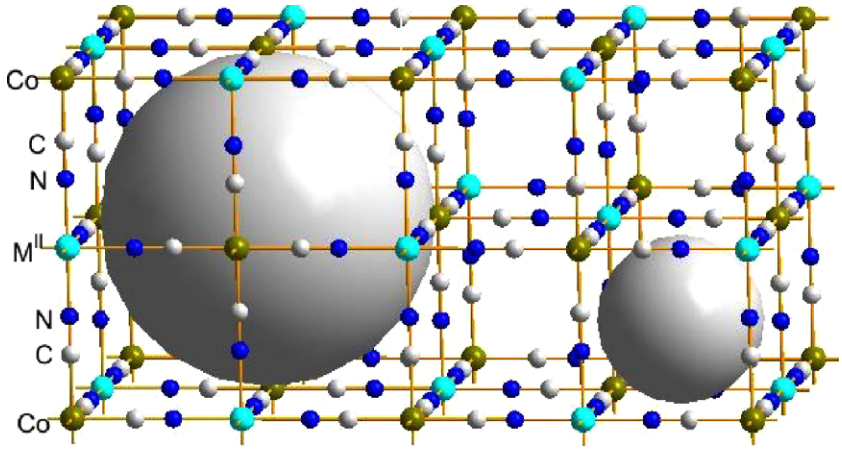

Fig. 1. Porous network for the cubic phases. The larger pores created by vacancies of the molecular block $[M(CN)_6]$ remain communicated by the interstitial free space (windows).

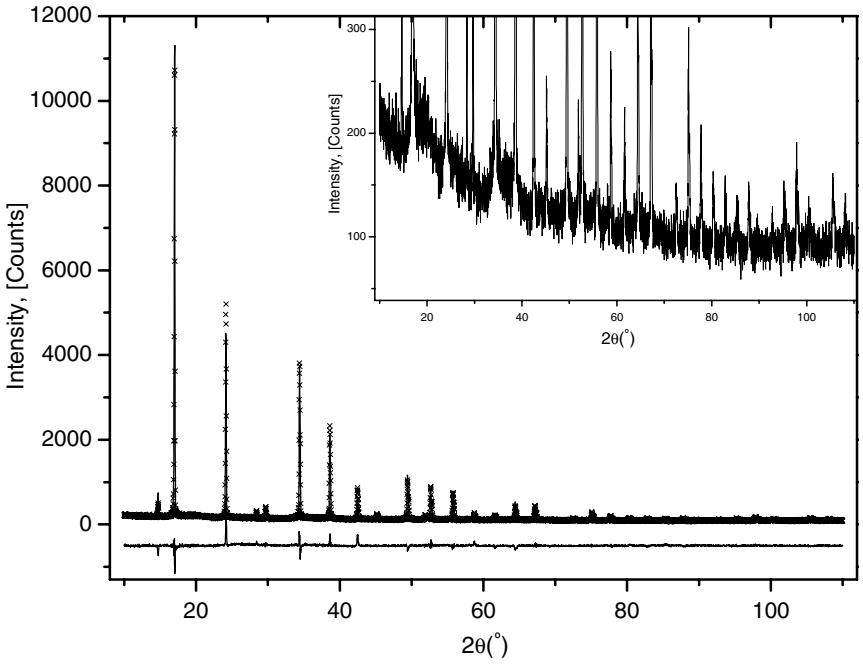

Fig. 2. Experimental and fitted XRD powder patterns and their difference for manganese hexacyanocobaltate(III). Inset: Sinuous background due to a diffuse dispersion contribution from the metal centers outside their ideal sites.

samples was estimated. The obtained values (in Å) are: Cu (8.33), Co (8.43), Mn (8.44), Cd (8.47), Ni (8.50) and Zn (8.50).

The smallest cell edge (10.062(1) Å) within the studied family of compounds corresponds to the copper complex salt. Since the unit cell edge corresponds to the T—N≡C—Co–C≡N–T chain length, such small cell edge value indicates that the copper and cobalt atoms are involved in a particularly strong interaction through the CN bridges. This strong interaction was attributed to the ability of the CN group to donate electron from its 5σ orbital, which has certain antibonding character, and to the copper atom capability to accept that charge in its 3d hole to attain an electronic configuration close to $3d^{10}$. This hypothesis is supported by Mössbauer and magnetic measurements for the iron analogues [34]. As will be discussed below, the reinforcement of the Cu–N bond is accompanied of a particularly weakening for the Cu–OH_2 interaction. This weak interaction of the copper atom with the coordinated waters is probably responsible for the low hydration degree observed for the copper salt (Table 1). Weakly bonded coordinated water molecules have low ability for the stabilization of non-coordinated waters within the pore through hydrogen bridges formation. An interesting fact is the very small deviation for the copper atom from the ideal position (Table 1). It seems that in the average Fm-3m structure, the copper atom behaves as a metal linked to four equatorial NC groups plus two weakly bonded axial waters. In such

Table 1
Cell edge values, metals deviation (<δ>) from their ideal positions for hydrated cubic phases, Rietveld refinement agreement factors (*R*), and cell contraction on dehydration

Compound[a]	Cell edge, Å	$<\delta>_{Co}$, Å	$<\delta>_{T}$, Å	R_{exp}	R_{wp}	R_B	Crystallite size, Å	Cell contraction, Vol.%
$Mn_3[Co(CN)_6]_2\cdot 13H_2O$	10.4211(1)	0.0105(2)	0.0249(3)	7.7	10.7	7.9	676	5
$Co_3[Co(CN)_6]_2\cdot 14H_2O$	10.2202(1)	0.0132(2)	0.0027(2)	9.4	11.0	8.3	175	4
$Ni_3[Co(CN)_6]_2\cdot 14H_2O$	10.162(1)	0.0240(3)	0.0301(2)	9.3	12.8	14.0	105	[b]
$Cu_3[Co(CN)_6]_2\cdot 10H_2O$	10.0621(2)	0.0013(2)	0.007(2)	3.7	4.3	9.3	279	3
$Zn_3[Co(CN)_6]_2\cdot 13H_2O$	10.2632(1)	0.008(4)	0.007(2)	12.5	16.9	11.3	734	6
$Zn_3[Co(CN)_6]_2$ (hex.)	a: 12.4847(3) b: 12.4847(3) c: 32.756(1)	–	–	3.9	7.5	7.4	–	–
$Cd_3[Co(CN)_6]_2\cdot 13H_2O$	10.591(1)	0.0130(2)	0.0117(2)	6.9	11.0	8.5	366	5

[a] The reported hydration degree was estimated from the TG curves.
[b] The anhydrous Ni complex produces an XRD powder pattern with broad peaks hindering a reliable estimation of the cell contraction.

configuration of ligands, the copper atom will be sited approximately on the equatorial plane, with only a small deviation from the ideal position. A similar coordination environment for copper has been observed in orthorhombic (Amm2) copper nitroprusside (four equatorial NC ligands and two axial waters) [35]. However, a most probably configuration of ligands for copper(2+) in hexacyanocobaltate(III), related to the Fm-3m structure, corresponds to a pseudo-tetrahedral environment of NC groups plus two weakly bonded water molecules, but with the copper atom sited close to the ideal (0, 0, 1/2) position. With the exception of copper, the local distortion for the metal approximately follows the order of its polarizing power, Ni > Co ~ Zn > Mn > Cd [36].

When the metal adopts a tetrahedral coordination with the N ends, a porous structure free of vacancies and of coordinated waters is obtained. The twelve N coordination sites provided by the two molecular blocks in the formula unit $T_3[Co(CN)_6]_2$,are sufficient to saturate the coordination environment for the three T atoms involved. This framework was observed for a modification of zinc cobalticyanide. This compound appears as dimorphic, cubic (Fm-3m) and rhombohedral (based on a hexagonal cell). The rhombohedral modification was observed when the cubic phase was dehydrated at relatively high temperature, ~90 °C, or when its synthesis was carried out from hot solutions. According to the XRD powder pattern, the rhombohedral phase crystallizes in the R-3c space group reported for Zn ferrocyanide [37]. The crystal structure of this last compound was used as starting model for the structural Rietveld refinement of the rhombohedral phase. In Table 1 the unit cell parameters calculated for this Zn phase are reported. The structure of the R-3c phase is more compact than that of the cubic modification. Their respective estimated densities, in g/cm^3, are ρ (R-3c): 1.408 and ρ(anhydrous Fm-3m): 1.278. The 3D porous framework of the rhombohedral phase is formed by ellipsoidal (elongated) cavities (Fig. 3) of ca. $5.1 \times 12.7 \times 8.3$ Å. These cavities remain communicated by windows of ca. 3.9×5.2 Å. This phase is hydrophobic, which suggests that its surface has a low electric field gradient (a practically non-polar surface). The ^{57}Fe Mössbauer spectrum, at room temperature, of the analogue rhombohedral zinc ferricyanide is an unresolved doublet with values of isomer shift (δ) and quadrupole splitting (Δ) of 0.111(6) mm/s and 0.236(3) mm/s, respectively [38]. This low value of Δ indicates that the iron nucleus is sensing a low electric field gradient in its environment. The rhombohedral zinc ferricyanide is also an anhydrous phase [38].

The cubic phase of zinc cobalticyanide is only stable in a wet atmosphere. Its prolonged aging, at room temperature (weeks) in partially dried air (below 70% of relative

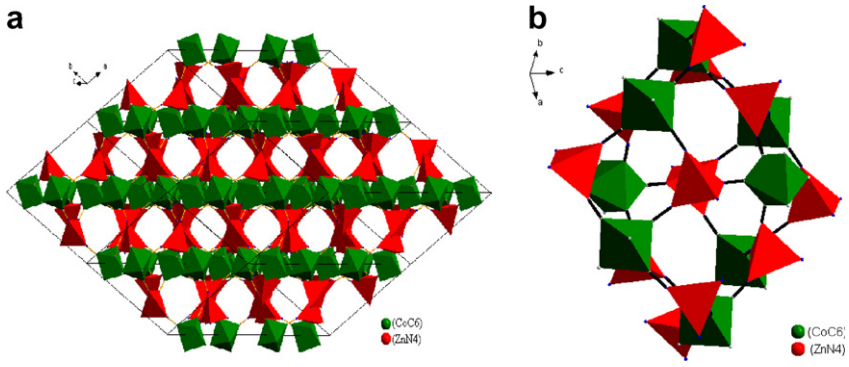

Fig. 3. (a) Porous framework of hexagonal Zn cobalticyanide formed by interconnected cavities. This structure is free of vacancies and the metal centers have saturated their coordination environment. (b) An isolated cavity where the cavity windows can be appreciated.

humidity), results in a mixture of hydrated (Fm-3m) and anhydrous (R-3c) phases. The vacuum dehydration of the cubic phase, even at room temperature, leads to a partial structural transformation (discussed below). The dimorphic nature of zinc cobalticyanide has usually been ignored, even in studies carried out under conditions where its structural transformation could be present [4,5].

IR spectroscopy provides useful information on the electronic structure of the studied compounds [39]. It is well known that cyanide at its *C* end behaves as a very strong ligand resulting in low spin electronic configuration for the metal in the molecular block $[M(CN)_6]$. At the N end it forms bond with more ionic character and, in consequence, the outer metal is usually found in a high spin state [40]. The IR spectra of the studied compounds are composed of three absorption bands from vibrations related to the octahedral $[Co(CN)_6]$ structural unit, ν(CN), δ(CoCN), ν(CoC), and those from the crystal water, $\nu(H_2O)$ and δ(HOH). In Table 2 the frequency values of these bands in the studied samples are collected. No rocking, $\rho(H_2O)$, and wagging, $w(H_2O)$, vibrations of bridged water molecules, which fall in the 900–700 cm^{-1} region [41], were observed in the studied materials. This indicates that all the coordinated water remains linked to only one coordination center. The stretching vibration of coordinated water in hexacyanometallates is usually observed as sharp bands around 3550 cm^{-1} but strongly overlapped with the broad absorption band due to that motion from the hydrogen bonded waters [39,41]. In cobalticyanides the ν(CoC) vibration usually falls below 400 cm^{-1} and it was not observed with the IR spectrophotometer used. The ν(CN) frequency is particularly high for the hexagonal modification of the Zn complex salt, 2203 versus 2188 cm^{-1} for the cubic phase. This was attributed to a stronger metal-ligand interaction for the tetrahedral coordination. An unusually high frequency of the ν(CN) vibration was also observed for copper cobalticyanide (2189 cm^{-1}), but in this case it is related to the above discussed strong Cu–N interaction. Such high CN stretching frequency for copper correlates with the observed behavior for other analogue salts [34].

The above discussed structural data reveal that the pore size and pore windows of this family of compounds depend on the metal that serves to link the N ends of neighboring octahedral blocks. In the cubic structure the metal is always found at the pore surface, six metal atoms per pore. In the rhombohedral zinc phase the surface is free of metal centers.

3.2. Dehydration process and thermal stability

All the studied compositions lose the crystal water at temperatures below 100 °C. Then the anhydrous phase remains stable up to 250 °C (Fig. 4). From the weight loss the sample hydration degree was estimated (Table 1). These compounds contain a large amount of hydrogen bonded water, from 5 to 8 molecules per formula unit, depending on the metal involved. The loss of these water molecules begins at relatively low temperature and even at room temperature, if the sample is maintained under a N_2 flow or in vacuum. On heating, all the crystal water evolves through a practically continuous process independently of its nature (coordinated or non-coordinated). On the evolution of the weakly bonded water molecules (non-coordinated), also a fraction of the coordinated ones abandon the solid, probably through a cooperative process, resulting in a TG curve without definite intermediate inflections. In the derivative curve (not shown) only a broad peak with its centre at the temperature of maximum dehydration rate appears. This temperature, of maximum weight loss, follows the order: Ni(95) > Mn(90) > Co(80) > Cd(75) > Cu(65) > Zn(38) which, with the exception of Cu and Zn, correlates with the reported metal polarizing power(Ze/r^2) [36]. The particularly strong interaction of the copper atom with the CN groups appears as responsible for the relatively low dehydration temperature for the copper complex salt [34]. In the case of Zn, the low dehydration temperature was ascribed to the trend of this metal to adopt a tetrahedral coordination forming the anhydrous rhombohedral phase.

When the heating was carried out in vacuum ($<10^{-2}$ Torr), the compounds were found to be anhydrous at 80 °C, and in the case of the Zn complex even at 30 °C. From these results, for the adsorption experiments all the samples were dehydrated at 80 °C in vacuum (10^{-2} Torr) during 4 h. The exception corresponded to the Ni complex, which required a higher temperature, ~105 °C, to obtain an anhydrous sample.

Table 2
Frequency (in cm^{-1}) of IR absorptions of the studied hexacyanocobaltates(III)

Compound	$\nu(H_2O)$	ν(CN)	δ(HOH)	δ(CoCN)
$Mn_3[Co(CN)_6]_2\cdot xH_2O$	3651; 3420(S,Br)	2165	1609; 1664(Sh)	451
$Co_3[Co(CN)_6]_2\cdot xH_2O$	3645; 3413(S,Br)	2173	1608; 1648(Sh)	458
$Ni_3[Co(CN)_6]_2\cdot xH_2O$	3644; 3399(S,Br)	2180	1609; 1670(Sh)	462
$Cu_3[Co(CN)_6]_2\cdot xH_2O$	3661; 3422(S,Br)	2189	1604; 1684(Sh)	468
$Zn_3[Co(CN)_6]_2\cdot xH_2O$	3651; 3449(S,Br)	2188	1615	464
$Zn_3[Co(CN)_6]_2$[a]	–	2203	–	445
$Cd_3[Co(CN)_6]_2\cdot xH_2O$	3640; 3483(S,Br)	2163	1611; 1664(Sh)	435

S: strong; Br: broad; Sh: shoulder.
[a] Anhydrous rhombohedral phase.

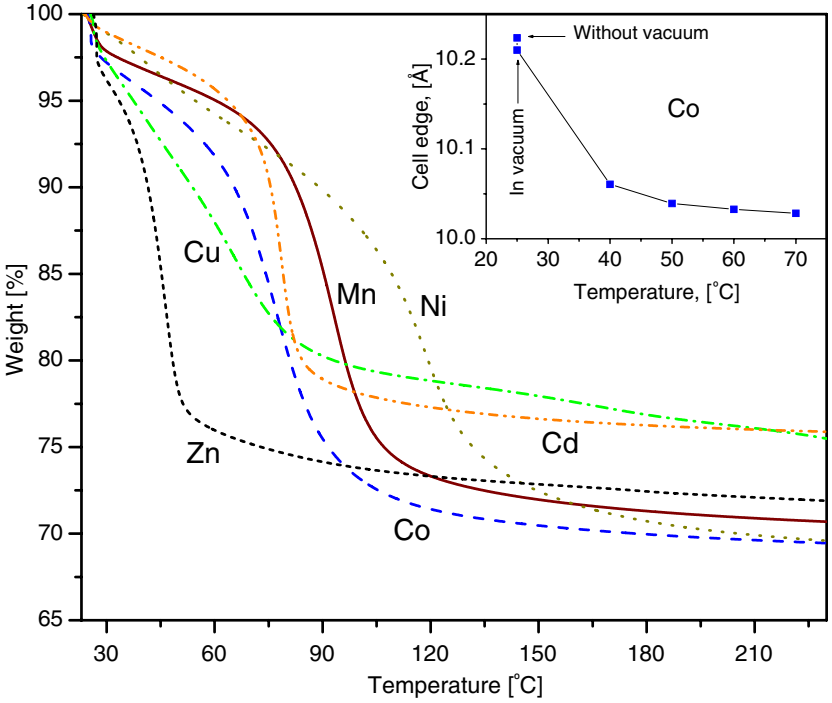

Fig. 4. TG curves (dehydration region) of the studied materials (cubic phases) recorded in high-resolution mode. These compounds lose the crystal water below 100 °C and then remain stable up to 250 °C. Coordinated and non-coordinated waters evolve through a practically continuous process. Inset: Cell contraction for the cobalt complex on the crystal water removal, estimated from XRD powder patterns recorded in vacuum at different heating temperatures.

Even for the most polarizing cation, Ni^{2+}, the estimated number of water molecules per formula unit is 14. It seems that this is the maximum number of water molecules that can be accommodated within a large pore. However, according to the molar volume of liquid water, 18.06 mL/mol, in a volume of 603 $Å^3$ (considering an octahedral pore of 8.45 Å of edge), up to 20 water molecules could be accommodated. This suggests that the water structure within the pore is slightly different to that expected for its liquid state or a smaller free space is really available for the water molecules. This last option could be attributed to repulsive interactions of the water oxygen atom with the negative charge on the –C≡N– bridges. The smaller hydration degree obtained for the Cu^{2+}, Zn^{2+} and Cd^{2+} salts was related to a weak interaction of these metals with the coordinated waters which reduces the stabilization energy for the hydrogen bonded waters within the pore.

With the exception of the cubic Zn complex, the remaining compositions preserve their crystal structure when the crystal water is removed by a soft heating. For the anhydrous cubic phases a cell contraction of about 4% of cell volume reduction was observed (see Table 1, Fig. 4 inset). This cell contraction is detected as peak shift to higher 2θ values in the recorded XRD powder patterns (Fig. 5). Such cell contraction is accompanied of certain structural disorder observed as peaks broadening (Fig. 5). An analogue structural effect on dehydration has been reported for other porous cyanometallates [3].

Coordinated and non-coordinated waters evolve, from the larger pores, without disrupting the crystalline network but favoring a stronger interaction among the metal centers through the CN bridges. When the coordinated waters are removed, all the interaction of the metal is with the CN groups. This leads to an increase in the charge subtraction

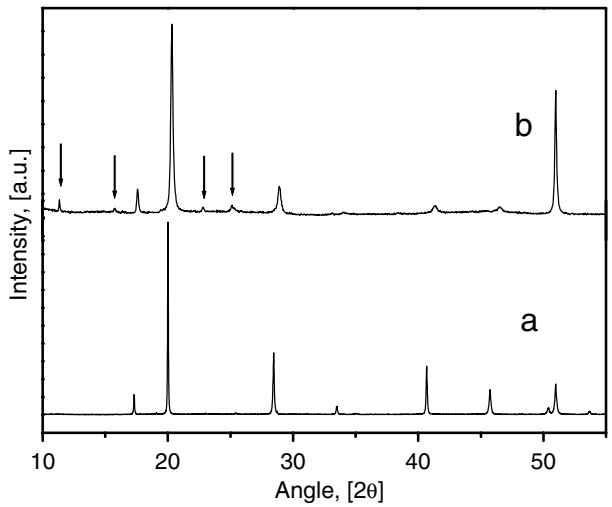

Fig. 5. XRD powder patterns of hydrated (a) and anhydrous (b) Zn cobalticyanide (cubic phase). On the water removal several effects are observed: (1) a unit cell contraction, (2) a peak broadening; (3) increase of the diffuse dispersion contribution; (4) formation of a minor fraction of the rhombohedral phase (indicated by arrows). The dehydration process was carried out in vacuum (10^{-5} Torr) at 30 °C.

from the ligands through their 5σ orbitals and also to a higher induced π-back donation from the cobalt atom towards the CN groups. These two coordinated effects contribute to a shorter T–N≡C–Co–C≡N–T chain length for the anhydrous sample. Even the evolution of the hydrogen bonded water molecules leads to a small but measurable cell contraction (Fig. 4, inset) but without a remarkable effect on the appearance of the XRD pattern. The mentioned peak broadening on the sample dehydration is accompanied of certain decrease in the peak intensity and of an increase in the diffuse dispersion contribution to the pattern background. Such changes in the XRD pattern have their origin in the local variation around the metal when the coordinated waters are removed. In the anhydrous sample a high ability of the metal at the pore surface to participate in interactions with guest molecules within the pores can be anticipated, particularly through electrostatic interactions.

The Zn complex salt dehydrates under vacuum at relatively low temperature (~30 °C) preserving the cubic structure with a minimum of rhombohedral phase formation (Fig. 5). When this anhydrous cubic phase was maintained at this temperature (days), a progressive conversion into the rhombohedral structure was observed.

The IR spectroscopy results are consistent with the XRD data. On dehydration the skeletal vibrations ν(CN) and δ(Co–C≡N) are preserved with only small shifts relative to the initial absorption frequencies. The exception corresponds to the Zn cubic phase where the heat induced structural transformation is easily detected through a pronounced frequency shift in the ν(CN) vibration (mentioned above). IR spectra of the evolved gases on heating correspond to water vapor except during the complex decomposition stage (above 250 °C) where absorption bands of C_2N_2 are detected. The appearance of C_2N_2 is related to a partial reduction of the metals (M = Co, T) by the released CN^- ligands, according to: $M^{n+} + CN^- \rightarrow M^{(n-1)+} + 1/2C_2N_2$ [38,42].

Water is a polar molecule and the material dehydration temperature and hydration degree can be taken as indicator of the electric field gradient that water senses at the pore surface. According to the above discussed TG data, the metal determines the electric field gradient at the pore surface and also the material interaction with guest-molecules (to be discussed below). Cobalticyanides have a relatively large region of stability as anhydrous phase, up to 250 °C, before their thermal decomposition, which is an attractive feature for potentials applications of this family of porous materials.

3.3. Water vapor adsorption isotherms

The water vapor adsorption complements the above discussed results derived from the TG data but, also reveals fine structural details not detected using XRD. Fig. 6 shows the water vapor adsorption isotherms for all the studied compounds, except for the rhombohedral Zn phase which is hydrophobic. These isotherms are typical of microporous structures [43]. For Ni, Co and Mn, the most polarizing metals, the adsorption of coordinated water molecules proceeds through relatively strong interaction, leaving a very low residual pressure (below 0.1 Torr) to be measured with the equipment used. In these cases, the adsorption isotherms provide information on the whole sample adsorption capacity and also on the adsorption process of weakly bonded (non-coordinated) water molecules. However, they fail to shed light on the guest–host interactions in the adsorption domain of coordinated waters and even for the water molecules stabilized by formation of strong hydrogen bridges with the coordinated ones. This fact is more pronounced for Ni where a large fraction of the non-coordinated waters are also firmly bonded. A strong metal-water interaction leads to an increase in the coordinated water protons ability to form hard hydrogen bonds. In this sense, Mn^{2+}, a metal with an intermediate polarizing power, represents the limit case where the first experimental points of the adsorption isotherm correspond to the adsorption of the most energetic hydrogen bonded water molecules (Fig. 6). For Cd, which is a bigger metal, the recorded isotherm contains information on the adsorption of both coordinated and non-coordinated waters, and also for Cu and Zn but due to different reasons (already mentioned).

The water adsorption isotherms show a positive slope in the region of relative pressures above 0.4, even for measurements carried out several hours after the water dosing (large equilibrium times). This could be explained as due to certain energy consumption by the solid during the adsorption event. This fact is probably related to a framework swelling during the adsorption process, increasing the available volume to allow the accommodation of new

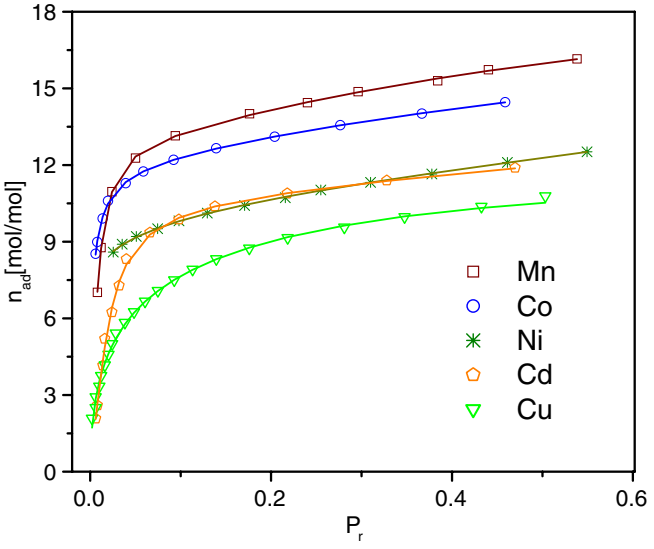

Fig. 6. Water vapor adsorption isotherms for cubic hexacyanocobaltates (III), $T_3[Co(CN)_6]$, recorded at 30 °C. These isotherms reveal certain dependence of the porous framework properties on the assembling metal (T) used.

water molecules within the pores. In addition, the TG curves in the region of dehydration do not correspond to an isothermic process, even for data recorded in a high-resolution experiment (Fig. 4). This suggests that in both, water desorption and adsorption processes the solid–fluid interaction changes, the last water molecules to be removed (or the first ones to be adsorbed) feeling the strongest interaction with the solid surface. This is equivalent to a change in the solid during these processes, which agrees with the observed cell contraction on dehydration. As already discussed, even the removal of non-coordinated water has certain contribution to the cell volume contraction (Fig. 4, inset). On the water adsorption, the inverse process, the cell expansion, is expected.

The adsorption of water in the anhydrous cubic Zn salt shows a unique behavior within the studied family of compounds (Fig. 7). Its isotherm appears as a sigmoidal type curve. The adsorption of the first water molecule (coordinated) requires of certain relative pressure (threshold) of water vapor to proceed. Then, from the adsorption of the second water molecule, the curve shows an inflexion and finally hydrogen bonded waters (non-coordinated) are adsorbed through a process similar to that observed for cadmium. It seems that in the anhydrous cubic phase the Zn atom adopts a pseudo-tetrahedral coordination with certain relative stability. At least a water molecule per Zn atom is required to perturb that state and to allow the adsorption of the second coordinated water molecule. Once the octahedral coordination around the Zn atom has been re-established the pore filling with hydrogen bonded waters is observed. This could explain the detected delay, in the pressure scale, for the water isotherm of this compound, effect not observed for the Cd salt, for instance. Such

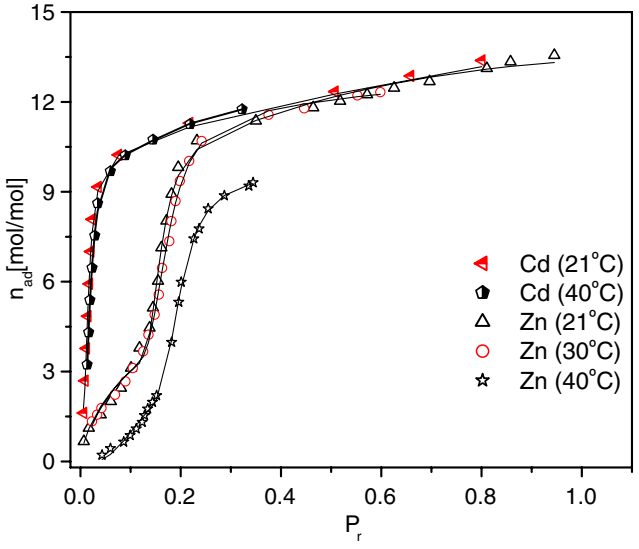

Fig. 7. Water vapor adsorption isotherms for Cd and Zn hexacyanocobaltates(III), $Cd_3[Co(CN)_6]$ and $Zn_3[Co(CN)_6]$ (cubic phase), recorded at different temperatures. For the Cd salt, the adsorption isotherm is temperature insensitive, even at 40 °C, behavior not observed for the Zn one.

atypical behavior for the Zn salt can not be attributed to presence of the rhombohedral modification. Pure rhombohedral Zn phase is a hydrophobic material and its transformation into the cubic structure (hydrophilic) was not observed during the time commonly used to obtain the water adsorption isotherm (two days).

The adsorption of water in the cubic Zn salt was studied at different temperatures (Fig. 7) and always the same sigmoidal type curve was obtained. The mentioned inflexion after the adsorption of the first water molecule is easily observed for the isotherm recorded at 40 °C. A higher thermal energy reduces the binding energy of the water molecule to the metal and a higher chemical potential (water pressure) to change the Zn atom coordination environment is required. According to XRD, at this temperature a fraction of the cubic phase transforms into the rhombohedral one (Fig. 5), particularly 18% for the sample used in the adsorption experiment (estimated from the reduction in the maximum adsorption capacity). It seems that the kinetic energy contribution, due to a higher temperature, favors the accommodation of the Zn atom in the tetrahedral coordination, overcoming the energy barrier between the pseudo-tetrahedral and the tetrahedral configurations. The change of ligands configuration around the zinc atom involves the movement of a large number of atoms. This could explain why it has a relatively low kinetics, at least at 40 °C. The estimated 18% of phase conversion corresponds to a sample maintained 120 h (5 days) at 40 °C. On re-hydration, from the anhydrous cubic phase, the octahedral coordination of the Zn atom is restored at expense of the adsorption energy of coordinated waters.

The obtained water vapor adsorption isotherm for the Cu salt results particularly interesting because it complements the above discussed evidence for a weak copper atom interaction with its coordination waters. Since copper (2+) and nickel (2+) have similar polarizing power [36], the expected interactions of these two metals with the coordination waters must be very similar. However, from the recorded adsorption isotherms (Fig. 6) a quite different behavior was observed. Copper behaves as cadmium, and even, compared with this last metal, for the former one a weaker interaction with the coordination waters corresponds. Cadmium (2+) is the biggest atom within the studied series of T metals, with the lowest polarizing power [36].

The water adsorption data were evaluated using the DA model (Eq. (1)). The results are summarized in Table 3. Some of these isotherms (Cu, Cd) require two fitting regions in Dubinin coordinates to be properly fitted. This was ascribed to the different nature of the adsorbed water molecules, coordinated and non-coordinated. To the first region corresponds a large energetic homogeneity, a large value for the heterogeneity parameter "n" in the DA model, and E_0 above 10 kJ/mol, while the second domain is characterized by a smaller value for "n" and with E_0 below 10 kJ/mol (Table 3). This small "n" value was interpreted as due to a variation in the guest–host interactions during the adsorption of the weakly bonded water

Table 3
Results derived from the H_2O, N_2 and CO_2 adsorption isotherms fitting according to the Dubinin model (n_p, the limiting amount adsorbed filling the micropores; E_0, characteristic energy; n, heterogeneity parameter; V_p, pore volume)

Complex salt	Adsorbate	n_p, mol/mol	E_0, kJ/mol	n	V_p, cm^3/g
$Mn_3[Co(CN)_6]_2 \cdot 14H_2O$	H_2O	12.6 ± 0.7	13.5 ± 0.8	5.2 ± 0.6	0.383 ± 0.021
		4.7 ± 1.3	3.8 ± 0.5	1.4 ± 0.4	0.143 ± 0.039
	N_2	7.70 ± 0.02	16.2 ± 0.5	1.01 ± 0.03	0.448 ± 0.012
	CO_2	3.90 ± 0.04	10.64 ± 0.04	2.43 ± 0.02	0.281 ± 0.003
$Co_3[Co(CN)_6]_2 \cdot 14H_2O$	H_2O	12.0 ± 0.5	17.8 ± 0.4	3.3 ± 0.2	0.357 ± 0.004
		4.0 ± 0.7	3.5 ± 0.5	1.3 ± 0.3	0.117 ± 0.021
	N_2	6.66 ± 0.03	14.0 ± 0.4	0.92 ± 0.03	0.381 ± 0.002
	CO_2	3.17 ± 0.03	10.94 ± 0.05	2.30 ± 0.02	0.224 ± 0.002
$Ni_3[Co(CN)_6]_2 \cdot 14H_2O$	H_2O	16.1 ± 0.3	23.7 ± 0.5	0.50 ± 0.02	0.482 ± 0.009
	N_2	–	–	–	–
	CO_2	2.56 ± 0.04	11.99 ± 0.09	2.50 ± 0.04	0.181 ± 0.003
$Cu_3[Co(CN)_6]_2 \cdot 11H_2O$	H_2O	11.0 ± 0.1	10.70 ± 0.07	1.67 ± 0.04	0.322 ± 0.003
	N_2	4.18 ± 0.06	14.8 ± 0.7	0.69 ± 0.05	0.234 ± 0.003
	CO_2	3.12 ± 0.05	12.35 ± 0.08	2.96 ± 0.06	0.202 ± 0.001
$Cd_3[Co(CN)_6]_2 \cdot 13H_2O$	H_2O	7.3 ± 0.8	10.5 ± 0.1	9.2 ± 1.3	0.171 ± 0.019
		6.7 ± 0.8	8.5 ± 2.3	0.7 ± 0.3	0.157 ± 0.019
	N_2	6.15 ± 0.03	21.0 ± 1.2	0.90 ± 0.04	0.276 ± 0.013
	CO_2	4.10 ± 0.2	10.22 ± 0.27	2.5 ± 0.1	0.227 ± 0.010
$Zn_3[Co(CN)_6]_2 \cdot 13H_2O$	H_2O	5.9 ± 0.6	7.3 ± 0.5	1.8 ± 0.2	0.172 ± 0.017
		6.6 ± 0.5	4.59 ± 0.03	10 ± 1	0.193 ± 0.013
	CO_2	3.41 ± 0.05	9.35 ± 0.02	2.27 ± 0.02	0.234 ± 0.003
$Zn_3[Co(CN)_6]_2$ (rhomb.)	N_2	5.48 ± 0.01	8.4 ± 0.2	1.38 ± 0.04	0.305 ± 0.006
$Zn_3[Co(CN)_6]_2$ (rhomb.)	CO_2	3.96 ± 0.06	9.23 ± 0.47	2.31 ± 0.02	0.272 ± 0.004

For Mn, Co, Zn, Cd the water adsorption isotherms were fitted using two fitting regions. To obtain the total V_p value the partial pore volumes from these two regions must be added.

molecules. The adsorption of these last waters has a more heterogeneous character and involves less energetic interactions. The value of 10 kJ/mol for E_0represents certain expected upper limit for the stabilization of water molecules in the adsorbed phase through hydrogen bonding interactions [44]. The adsorption of water in Cd, Cu and Zn complex salts is characterized by the lower values of E_0 due to the relatively weak interaction of these metals with the coordinated waters. This is notable for the case of the cubic Zn phase.

The hydration degree of the studied compounds, estimated from the limiting amount filling the micropores (n_p) results slightly higher than that obtained from TG curves (Tables 1 and 3). The adsorption isotherms were recorded until saturation in water vapor while the TG analyses were carried out on samples equilibrated at 80% of relative humidity, which could explain the observed difference. Under the adsorption experiment conditions water molecules could occupy all the material free space, probably also including the interstitial voids. The pore volume obtained for this family of compounds, estimated from the n_p value, falls in the 0.360–0.530 cm^3/g range (Table 3). This wide variation of pore volume suggests that in some compounds a fraction of the free space could remain unoccupied by water molecules. Another option, and the most probable, is an overestimation of the free space due to water adsorption on the external surface or on a mesoporous domain. No such variation is observed when the pore volume is estimated from the hydration degree derived from the TG curves (Table 3). For all the studied cobalticyanides approximately analogue values for the pore volume are expected, because the larger pores result from systematic vacancies of the elemental building unit. The estimated values of V_p are slightly higher than those found for microporous nitroprussides (0.322–0.376 cm^3/g) [7], and also higher than those reported for some zeolites (mordenite: 0.165 cm^3/g, clinoptilolite: 0.198 cm^3/g) [45]. The smaller estimated V_p value (0.360 cm^3/g), corresponds to the Cu compound. This was attributed to already-discussed unique bonding properties between the cupper atom and the CN ligands.

3.4. Nitrogen adsorption isotherms

Fig. 8 shows the nitrogen adsorption isotherms for the studied cobalticyanides. These isotherms were recorded using large equilibrium times, up to 100 hours per curve for copper for instance, to avoid kinetic effect in the obtained data. As already-mentioned, this family of materials has relatively small pore windows and for short equilibrium times a pronounced hysteresis between the adsorption and desorption events, at medium values of relative pressure, is observed. Under the used large measurement times, only for copper a slight hysteresis prevails

(Fig. 8). The small diffusion rate of N_2 during the pore filling is related to both a low measurement temperature (−196 °C) and the small window size. For Cu and Co, above 0.8 of relative pressure, the N_2 adsorption isotherm shows a marked hysteresis, which persists even for large equilibrium times. Such hysteresis was ascribed to capillary condensation in a mesoporous region. The nature of such mesoporous structure could be the aggregation of small crystallites. According to XRD, the smallest estimated crystallite size corresponds to these two complex salts (Table 1). Before that region of capillary condensation all the obtained isotherms reach a plateau corresponding to the maximum adsorbed amount filling the accessible micropores. The observed value of that plateau is different for each of the studied compounds (Fig. 8). This suggests that not all the larger pores are really accessible for the N_2 molecule (at −196 °C). It seems that the pore accessibility is controlled by the metal through its polarizing power (Ze/r^2). For the Ni compound, for instance, practically all the porous framework results inaccessible while for the Cu one, only a fraction of the whole free space becomes accessible to N_2. An analogue result has been reported for transition metal nitroprussides [7]. Such behavior in nitroprussides was attributed to the large polarizing power of the NO group, which deforms the environment of the iron atom in the $[Fe(CN)_5NO]$ block reducing the effective pore windows cross-section and hindering the pore filling with N_2. A similar effect could be present in the studied compounds but here modulated by the metal polarizing power. The porous framework of nickel ferricyanide has also been reported as inaccessible for N_2[3]. An additional structural factor in the pore accessibility to be considered is the cell contraction on cooling. The N_2 adsorption isotherms in the evaluated samples show certain positive slope in the region of medium values of relative pressure which was ascribed to a small solid expansion on the pore filling, an effect already discussed for the adsorption of water.

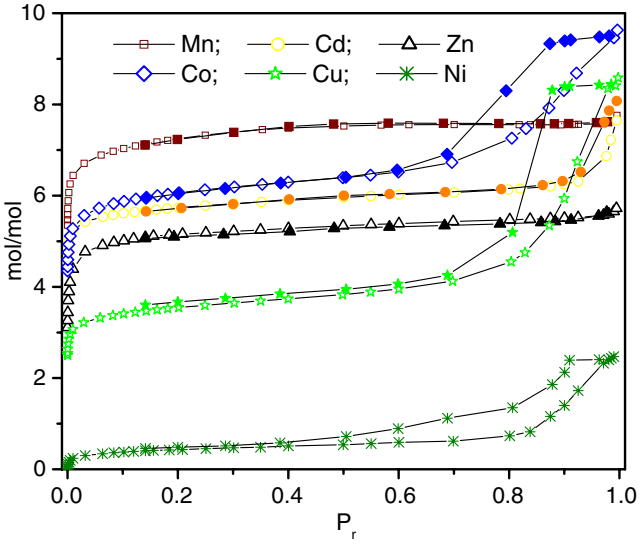

Fig. 8. N_2 adsorption isotherms for the studied family of compounds ($T_3[Co(CN)_6]$). These isotherms reveal a marked dependence of the porous network properties on the metal (T) used.

The inaccessibility of a fraction of the free space to N_2 in the studied cubic phases is evident comparing their adsorption isotherms with that obtained for the rhombohedral Zn phase. The pores of this last one remain communicated by relatively large windows and the framework shows a higher rigidity. However, this phase, with a smaller free space (a higher density), occupies an intermediate position between the cubic compounds, according to the adsorbed amount filling the pores (Fig. 8).

The control of the pore accessibility by the metal appears particularly interesting. Information on the nature of this effect can be obtained from Mössbauer spectra of ferricyanides analogues with different adsorbed species [25], different metals [46] and at different degree of pore filling [3]. The quadrupole splitting (Δ) in ferricyanides shows a monotonous dependence on the metal polarizing power, Cu(0.54) > Ni(0.50) > Co(0.43) > Zn(0.35) > Mn(0.27) > Cd(0.25) [36,46]. The value of Δ is sensing the metal environment deformation.

The N_2 adsorption isotherms were evaluated using the DA model. The resulting values of E_0, n and V_p are summarized in Table 3. The maximum adsorption, 7.7 mol/mol, was observed for the Mn salt. According to the molar volume of N_2 (34.67 ml/mol.), the adsorption of these 7.7 N_2 molecules requires a volume of 443 Å^3. This salt has 14 water molecules per formula unit for an estimated space occupied by these water molecules of 420 Å^3. This suggests that for a given cobalticyanide with high pore accessibility to the N_2 molecule, like the Mn salt, the nitrogen and water molecules sense similar free space. According to the estimated pore size (from XRD results), the expected pore volume for the Mn compound is close to 600 Å^3. It seems that the effective available space for the adsorption of N_2 and H_2O is significantly smaller. This effect is probably due to repulsive probe molecules interactions with C≡N electron cloud. The estimated pore volume, accessible to N_2, follows the order: Mn > Co > Zn > Cd > Cu > Ni. The calculated characteristic energy, E_0, shows a wide variation, from 8 to 21 kJ/mol, depending on the metal involved, with the lower value for the Zn salt and the upper limit for the Cd one. The interaction of the nitrogen molecule with the solid surface must be dominated by the adsorbate quadrupole moment interaction with the electric field gradient at the pore surface plus certain contribution from van der Waals interactions. Cd is a bigger atom where a quadrupole moment is more easily induced facilitating a stronger surface interaction with the N_2 molecule quadrupole moment (dispersive interaction). The inverse behavior is expected for the Zn atom because it has a smaller size and remains strongly bonded within a tetrahedral environment of N atoms. In addition, the rhombohedral phase has a rigid structure with practically all the electronic structure engaged in relatively strong chemical bonds, and a practically non-polar surface. For the Mn, Co and Cu salts intermediate values of E_0 were obtained

(Table 3). For the heterogeneity parameter, n, relatively low values were found. This suggests certain energetic heterogeneity in the guest–host interaction during the N_2 adsorption process. The first molecules to be adsorbed are stabilized through an interaction that involves the electric field gradient at the pore surface with the quadrupole moment of the N_2 molecule. Then, the pore filling continues in the absence of such interaction and through weaker guest-guest interactions between N_2 molecules. This situation is similar to that above discussed for the adsorption of water. The higher value of n, the most energetically homogeneous N_2 adsorption, was observed for the rhombohedral Zn phase, related to the nature of the pore surface in this structure (already discussed).

3.5. Carbon dioxide adsorption isotherms

The CO_2 adsorption experiments were mainly oriented to shed light on the pore accessibility in the studied materials. Fig. 9 shows the CO_2 adsorption isotherms recorded for the studied samples. These isotherms are typical of microporous structures indicating that the materials porous framework is really accessible to the CO_2 molecule, even for the Ni salt which was found to be inaccessible to N_2. This is an expected result. The CO_2 molecule has an elliptical form which allows its diffusion through the small pore windows of the studied materials. In Table 3 the results obtained from the fitting of the CO_2 adsorption isotherms combining the DA and LF models (Eqs. (1) and (2)) are reported. The maximum adsorption (n_p) in Eq. (1) was estimated by extrapolation of the fitted curve using the LF model (Eq. (2)). The n_p value shows a pronounced dependence on the metal, from 2.56 for Ni up to 4.10 for Cd. Such dependence was attributed to a modulation effect by the metal on the pore surface properties and on the pore

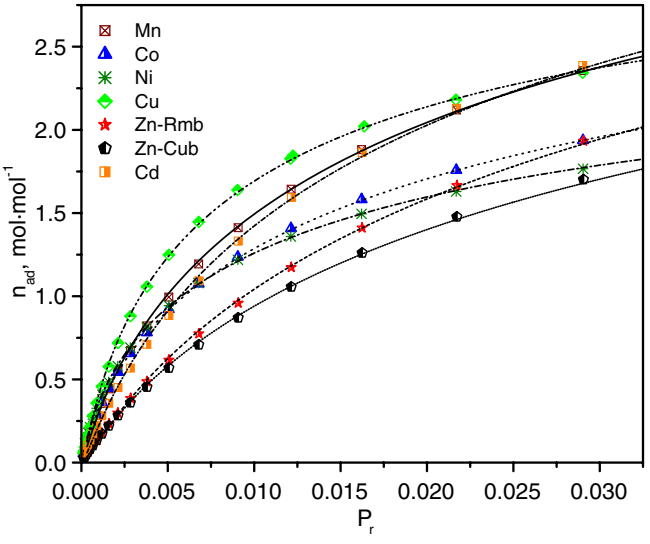

Fig. 9. CO_2 adsorption isotherms for the studied hexacyanocobaltates ($T_3[Co(CN)_6]$). These isotherms show certain dependence of the material properties on the metal (T) used to form the 3D network.

accessibility. The stabilization of the CO_2 molecule within the pore is probably related to two contributions, van der Waals forces and interaction of the molecule quadrupole moment with the electric field gradient at the pore surface, both are short distance interactions. The stronger probe-pore surface interaction (the larger E_0 value) was observed for Cu, the metal where the smaller pore diameter was estimated and where the CO_2 is more confined. This could explain that the stronger guest–host interaction corresponds to the copper complex salt. For Ni the interaction is also significantly strong but in this case the dominant stabilization mechanism is probably related to the large electric field gradient at the pore surface. At the opposite side the zinc salts are found (Fig. 9 and Table 3), particularly for the rhombohedral phase due to its practically non-polar pore surface and larger pore size, two factors that weaken the guest–host interaction for the CO_2 molecule within the pore. The remaining metals occupy an intermediate position according to the material-CO_2 molecule strength interaction.

All the interaction of the CO_2 molecule with the host solid is of physical nature. No variation in the IR spectra for the solid on the CO_2 adsorption was detected. This aggress with reported results for other families of porous cyanometallates [3,7,9,19].

According to the estimated value for the heterogeneity parameter, n, which remains above 2, the adsorption of CO_2 takes place under certain energetic heterogeneity. This could be related to the nature of the porous framework in the studied materials, a structure where certain randomly distribution of vacancies is expected. For porous carbons which show certain energetic heterogeneity for the adsorption, due to their non-regular structure, the reported values for this parameter (n) are close to 2 [21].

Because the measurement temperature (0 °C) is relatively near the critical temperature for CO_2 (31 °C), the calculated pore volume from the CO_2 adsorption is relatively low. Probably the CO_2 molecules only occupy a fraction of the structure free space due to the kinetic energy of the adsorbate which competes with its stabilization energy within the pore. According to the molar volume for CO_2, 42.9 mL/mol, within a large pore up to seven CO_2 could be accommodated but, the estimated n_p value (in mol/mol) (Table 3) remains below that upper limit.

3.6. The temperature invariability of the water vapor adsorption isotherms

The DA model used for the evaluation of the adsorption data is based in two postulates: (a) the temperature independence for the free energy related to the adsorption process (adsorption potential, A); (b) the validity of certain empirical dependence that relates the volumetric filling $\theta(n_{ad}/n_p)$ with the adsorption potential (A) according to a Weibull distribution ($\theta = \exp[-(A/E_0)^n]$) where E_0 and n are the characteristic energy and the heterogeneity parameter, respectively [21,22]. In order to shed light on

the validity of the first postulate in the studied systems, the water vapor adsorption isotherms were recorded at different temperatures between 20 and 40 °C. The independence of the adsorption isotherm on the measurement temperature is equivalent to the temperature independence for adsorption potential (A).

Fig. 7 shows the water vapor adsorption isotherms for Zn and Cd salts recorded at different temperatures. Within the studied family of compounds, in these two complex salts the weakest guest–host interactions, for the adsorption of water, were observed. In such compositions the higher temperature effect on the adsorption is expected. The adsorption isotherm estimated for the Cd salt remains without appreciable variation in the studied range of temperature. At a higher temperature the water vapor pressure (P_0) changes but for a given value of the relative pressure after the water dosing ($P_r = P_{eq}/P_0$), the amount of water vapor that is adsorbed does not change suggesting that the adsorption potential results temperature insensitive. This suggests that the guest–host interactions are sufficiently strong to be perturbed by a change in both the solid vibrational energy and the kinetic energy of the water molecule to be adsorbed. A temperature of 40 °C is relatively far from the observed temperature of maximum dehydration rate for the Cd salt (75 °C). However, for the Zn compound, where a significant fraction of its crystal water can be removed at low temperature, the corresponding adsorption isotherm is temperature insensitive only up to around 30 °C (Fig. 7). The adsorption isotherm at 40 °C shows a combined effect of structural transformation of a sample fraction plus certain temperature dependence for the adsorption potential. The formed fraction of rhombohedral phase reduces the water adsorption sample capacity because that new structure is hydrophobic. The temperature dependence of the adsorption potential is detected as a change in the resulting isotherm. At this temperature (40 °C), the adsorption of a given amount of water molecules requires of a higher relative pressure of water vapor, in contrast with the observed behavior for isotherms recorded at 21 and 30 °C. These results justify the water vapor adsorption data collection at a temperature of 30 °C for all the studied samples.

3.7. Estimated values for the adsorption work

Considering the temperature independence of the adsorption potential for the adsorption of water, the molar differential adsorption work was estimated directly from the experimental isotherm according to Eq. (3). Fig. 10 shows the characteristic curves for water adsorption. For Ni, Co and Mn only information on the energy related to the adsorption of non-coordinated waters can be obtained and the value estimated for the molar differential adsorption work (A) remains below 14 kJ/mol. Such high values of A are due to the large ability of water molecules coordinated to these metals to stabilize hydrogen bonded waters in their environment through hydrogen bonding interactions. For Cu, Cd and Zn, where the obtained data also include the adsorption of coordinated waters, the estimated value of adsorption work is only slightly higher, 16 kJ/mol as upper limit. This limit value reveals a relatively weak interaction of the metal with its waters of coordination. This is particularly true for the Zn salt (cubic phase) where the adsorption work for coordinated waters remains below 8 kJ.mol^{-1}. In this compound the adsorption of non-coordinated waters proceeds on an iso-energetic domain, dominated by adsorbate-adsorbate interactions with a minimum effect of the host structure, behavior not observed for the remaining compositions (Fig. 10).

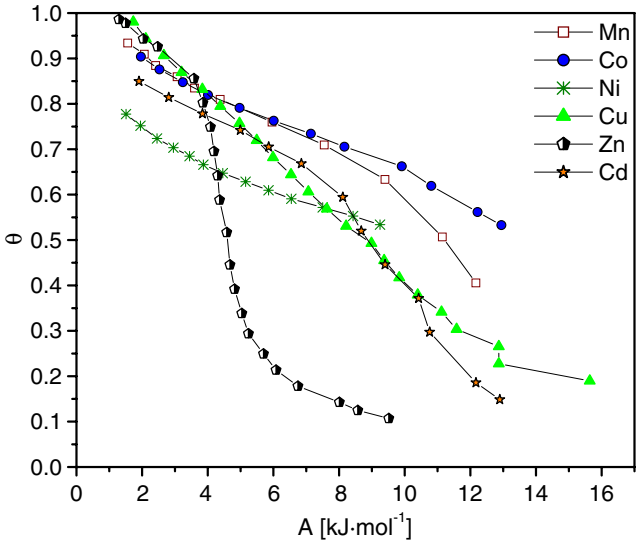

Fig. 10. Dependence of the fractional microporous volume filling (θ) on the adsorption potential (A) for the adsorption of water in the studied materials.

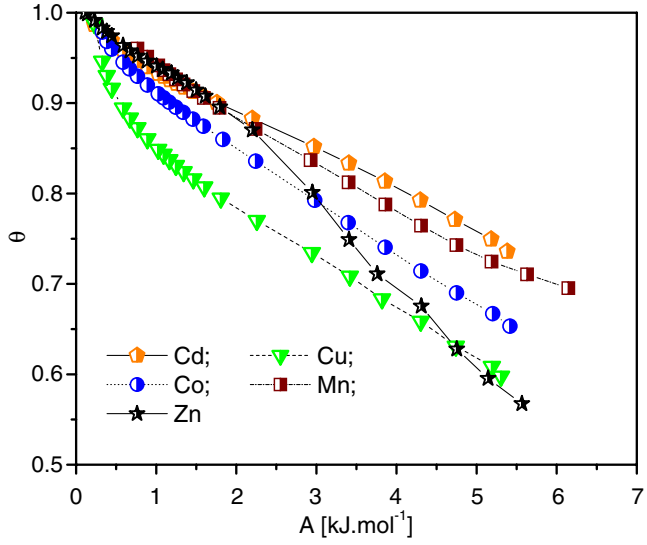

Fig. 11. Dependence of the fractional microporous volume filling (θ) on the adsorption potential (A) for the adsorption of N_2 in the studied family of compounds.

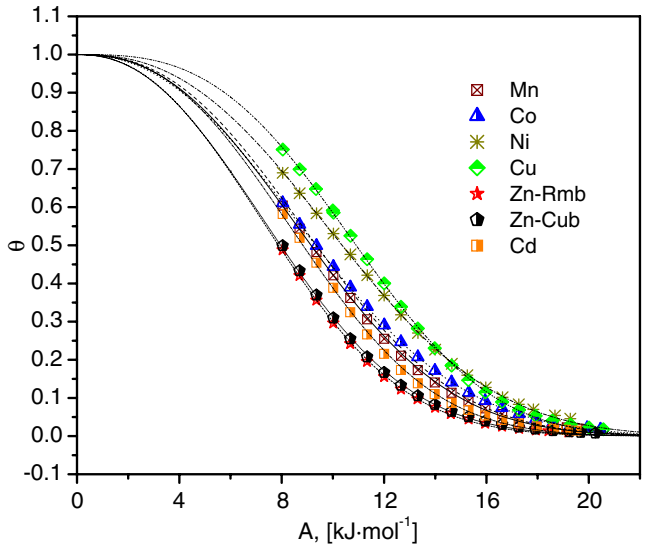

Fig. 12. Dependence of the fractional microporous volume filling (θ) on the adsorption potential (A) for the adsorption of CO_2 in the studied family of compounds.

The same formalism was used to estimate the adsorption work for N_2 and CO_2, under the hypothesis of validity of the above mentioned postulates. The adsorption of nitrogen involves adsorption works below 7 kJ/mol. (Fig. 11), and with a practically linear dependence on the volumetric filling, and approximately the same slope, except for the Zn salt. Such behavior agrees with the above discussed nature of the guest–host interactions for the N_2 adsorption. The adsorption of CO_2 is related to larger adsorption works involving A values close to 20 kJ/mol for the first molecules that are adsorbed (Fig. 12). It seems that the first CO_2 molecules to be adsorbed are sited on the pore surface of stronger electric field gradient or where they are highly confined involving large values for the adsorption work. Compared to N_2, the adsorption of CO_2 appears as a more favorable process.

4. Conclusions

Divalent transition metals hexacyanocobaltates(III) form a family of microporous compounds which behave as molecular zeolites with a tunable porous framework. Their pore volume, pore accessibility and adsorption potential appear modulated by the metal used to join the building block. In this family of compounds two typical porous structures, with different physical properties are found. For those frameworks based on a cubic unit cell the porous structure comes from systematic vacancies of the octahedral building block resulting in materials with polar surface. But, when the metal is Zn, which can also be tetrahedral coordinated to N atoms of the CN ligands, the resulting solid is dimorphic, cubic and rhombohedral. To the rhombohedral modification corresponds a smaller available free space but with larger pore size and pore windows. Their pores are also different in physical properties. Such diversity of properties could find some attractive applications. The studied compounds are free of exchangeable ions in the porous framework and, in consequence, without strong charge centers to provide a high stability to the guest species. With the exception of the rhombohedral modification of the Zn salt, which is anhydrous, all the studied compositions are obtained with a large amount of crystal water which can be removed by heating at relatively a low temperature below 100 °C, and then the anhydrous structure remain stable up to 250 °C.

Acknowledgments

The access to the LNLS synchrotron radiation facility (Brazil) through the research projects 3275 and 3276 (2005) is gratefully recognized. E.R. thanks the partial support from the CLAF-ICTP Small Grants Program. This research was partially supported by CONACyT (Mexico) through the Project SEP-2004-C01-47070. The authors thank E. Fresgoso-Israel from IIM-UNAM the TG data collection.

Appendix A. Supplementary data

The Supplementary Information includes: all the structural data derived from the crystal structure Rietveld refinement for the studied samples that include: the XRD powder patterns fitting, the obtained atomic positions, occupation and temperature factors and the estimated inter-atomic distances and bond angles. Structural information has also been deposited at ICSD Fachinformationszentrum Karlsruhe (FIZ) (email: crysdata@fiz-karlsruhe.de) with CSD file numbers: 416745: $Mn_3[Co(CN)_6]_2\cdot 14H_2O$; 416742: $Co_3[Co(CN)_6]_2\cdot 14H_2O$; 416746: $Ni_3[Co(CN)_6]_2\cdot 14H_2O$; 416743: $Cu_3[Co(CN)_6]_2\cdot 10H_2O$; 416744: $Zn_3[Co(CN)_6]_2\cdot 13H_2O$ (cubic); 416740:$Zn_3[Co(CN)_6]_2$ (rhombohedral); 416741: $Cd_3[Co(CN)_6]_2\cdot 13H_2O$. Supplementary Information associated with this article is available from the online version, at doi:10.1016/j.micromeso.2007.01.030.

References

[1] G. Boxhoorn, J. Moolhuysen, J.P.G. Coolegem, R.A. van Santen, J. Chem. Soc., Chem. Commun. (1985) 1305.
[2] K.R. Dunbar, R.A. Heintz, Prog. Inorg. Chem. 45 (1997) 283.
[3] J. Balmaseda, E. Reguera, J. Rodríguez-Hernández, L. Reguera, M. Autie, Micropr. Mesopor. Mater. 96 (2006) 222.
[4] S.S. Kaye, J.R. Long, J. Am. Chem. Soc. 127 (2005) 6506.
[5] K.W. Chapman, P.D. Southon, C.L. Weeks, C.J. Kepert, Chem. Commun. (2005) 3322.
[6] M.R. Hartman, V.K. Peterson, Y. Liu, S.S. Kaye, J.R. Long, Mater. Chem. 18 (2006) 3221.
[7] J. Balmaseda, E. Reguera, A. Gomez, J. Roque, C. Vazquez, M. Autie, J. Phys. Chem. B 107 (2003) 11360.
[8] J.T. Culp, C. Matranga, M. Smith, E.W. Bittner, B. Bockrath, J. Phys. Chem. B. 110 (2006) 8325.
[9] R. Martinez-Garcia, M. Knobel, E. Reguera, J. Phys.: Condens. Matter 18 (2006) 11243.

[10] S. Ferlay, T. Mallah, R. Ouahes, P. Veillet, M. Verdaguer, Nature 378 (1995) 701.
[11] S.M. Holmes, G.S. Girolami, J. Am. Chem Soc. 121 (1999) 5593.
[12] O. Sato, T. Iyoda, A. Fujishima, K. Hashimoto, Science 272 (1996) 704.
[13] S. Ohkoshi, K. Arai, Y. Sato, K. Hashimoto, Nat. Mater. 3 (2004) 857.
[14] W.E. Buschmann, J. Ensling, P. Gutlich, J.S. Miller, Chem. Eur. J. 5 (1999) 3019.
[15] D. Louer, R. Vargas, J. Appl. Crystallogr. 15 (1982) 542.
[16] J. Rodriguez-Carvajal, FULLPROFS 98 Program, Institute Leon Brillouin, Saclay, France, 1998.
[17] A.C. Larson, R.B.V. Dreele, GSAS: General Structure Analysis System, 2000.
[18] D.R. Lide (Ed.), CRC Handbook of Chemistry and Physics, 84th ed., 2003–2004.
[19] J. Balmaseda, E. Reguera, J. Fernandez, A. Gordillo, H. Yee-Madeira, J. Phys. Chem. Solids 64 (2003) 685.
[20] E. Reguera, J. Balmaseda, J. Rodríguez, M. Autie, A. Gordillo, H. Yee-Madeira, Porous Mater. 11 (2004) 219.
[21] M.M. Dubinin, in: D.A. Cadenheat (Ed.), Progress in Surface Science and Membrane Science, Academic Press, New York, 1975.
[22] F. Stoeckli, Russ. Chem. Bull. Int. Ed. 50 (2001) 2265.
[23] M.H. Simonot-Grange, J. Chim. Phys. 84 (1987) 1161.
[24] P. Cartraud, A. Cointot, A. Renaud, J. Chem. Soc., Faraday Trans. 1 (77) (1981) 1561.
[25] J. Balmaseda, E. Reguera, A. Gomez, B. Diaz, M. Autie, Micropor. Mesopor. Mater. 54 (2002) 285.
[26] B.P. Bering, V.V. Serpinski, Inst. Fiz. Khim., Moscow, Russ. Izvest. Akad. Nauk SSSR, Seriya Khim. 11 (1974) 2427.
[27] B.P. Bering, M.M. Dubinin, V.V. Serpinskii, J. Colloid Interf. Sci. 21 (1966) 378.
[28] R. Roque-Malherbe, Micropor. Mesopor. Mater. 41 (2000) 227.
[29] A. Ludi, A. Gudel, Struct. Bond. 14 (1973) 1.
[30] A. Ludi, H.U. Gudel, Helv. Chim. Acta 51 (1968) 2006.
[31] D.F. Mullica, W.O. Milligan, Acta Crystallogr. B 34 (1978) 3558.
[32] G.W. Beall, W.O. Milligan, Inorg. Chem. 16 (1977) 2715.
[33] R.D. Shannon, Acta Crystallogr. A 32 (1976) 751.
[34] E. Reguera, J. Rodríguez-Hernández, A. Champi, J.G. Duque, E. Granados, C. Rettori, Z. Phys. Chem. 220 (2006) 1609.
[35] A. Gomez, J. Rodríguez, E. Reguera, J. Chem. Crystallogr. 34 (2004) 893.
[36] Y. Zhang, Inorg. Chem. 21 (1992) 3889.
[37] P. Gravereau, E. Garnier, A. Hardy, Acta Crystallogr. B 35 (1979) 2843.
[38] R. Martinez-García, M. Knobel, E. Reguera, J. Phys. Chem. B 110 (2006) 7296.
[39] K. Nakamoto, in: Infrared and Raman Spectra of Inorganic and Coordination Compounds, John-Wiley & Sons, New York, Chichester, Brisbane, Toronto, Singapore, 1986, p. 484.
[40] A.G. Sharpe, in: P. Maitlis, F.A.G. Stone, R. West (Eds.), The Chemistry of Cyano Complexes of the Transition Metals, Academic Press, New York, 1976.
[41] A. Gomez, E. Reguera, Int. J. Inorg. Mater. 3 (2001) 1045.
[42] E. Reguera, J. Balmaseda, G. Quintana, J. Fernández, Polydedron 17 (1998) 2353.
[43] S.W. Sing, D.H. Everett, R.A.W. Haul, L. Moscou, R.A. Pierotti, J. Rouquerol, T. Siemienswska, Pure Appl. Chem. 57 (1985) 603.
[44] I.D. Brown, Acta Crystallogr. A 32 (1976) 24.
[45] D.W. Breck, in: Zeolites Molecular Sieves: Structure, Chemistry, and Use, John Wiley & Sons, New York, 1974.
[46] E. Reguera, J. Fernandez, Hyperfine Interact. 88 (1994) 49.